Journal of
Ceramic Science
and Technology

J. Ceram. Sci. Tech., 02 [02] 103-110 (2011)
DOI: 10.4416/JCST2011-00010
available online at: http://www.ceramic-science.com

Characterization of the Crystallization Behavior of Laser-Fused Transparent Microspheres with the Eutectic Composition Al_2O_3-Y_2O_3-ZrO_2 (AYZ)

C. Oelgardt[1], J. Günster[2], J. G. Heinrich[1]

[1]Clausthal University of Technology, Institute of Nonmetallic Materials, Department for Engineering Ceramics, 38678 Clausthal-Zellerfeld, Germany
[2]BAM – Federal Institute for Materials Research and Testing, Division 5.4 – Advanced Ceramics, 12203 Berlin, Germany

received March 9, 2011; accepted March 22, 2011

Abstract

Transparent microspheres with the eutectic composition 65 Al_2O_3-16 Y_2O_3-19 ZrO_2 (mol%) have been produced by laser fusing with a CO_2 laser. The influence of the starting material – not pre-calcined and pre-calcined – as well as the laser power on the resulting microspheres – was investigated. After fabrication, the microspheres were analyzed by means of XRD to quantify the amorphous content of the spheres as well as to identify the residual crystalline phases, with a laser granulometer to measure the particle sizes of the starting material and the resulting microspheres, with DSC to characterize the glass transition temperature and crystallization behavior, and with SEM to investigate the microstructure of the microspheres. The laser-treated materials consist of transparent and opaque beads as well as sintered particles. The amorphous amount in the samples was detected to be ~ 85 %. Based on these results transparent beads were collected and annealed over a range of temperatures to analyze the crystallization behavior.

Keywords: Eutectic ceramics, Al_2O_3-Y_2O_3-ZrO_2, laser processing, crystallization behavior, microstructure

I. Introduction

The development of ceramics for optical applications has been an interesting research area in recent years. The advantages in comparison to conventional glasses are better mechanical properties (i.e. hardness), higher temperature stability, thermal shock resistance and a higher refractive indices as well as light transmission in a wider spectral range. The transparent ceramics find application for example in optical systems like cameras or lasers and as armor materials.

To achieve the required transparency (which may change from application to application), the process and the raw materials are very important. On one hand small grain sizes are required and on the other hand a density very close to the theoretical density is necessary, which implies in most cases the use of nanopowders. The conventional way to produce transparent ceramics is the sintering process (pressureless or vacuum) followed by hot isostatic pressing (HIP) [1–3]. A second route to achieving transparent materials is rapid quenching from the melt to an amorphous system followed by controlled crystallization, which is the traditional glass-ceramic process [4–7].

Araki *et al.* [8] produced transparent nanosized ceramics with a diameter of about 3 mm in the system HfO_2-Al_2O_3-$GdAlO_3$ by means of solidification from the eutectic melt with cooling rates between 200 and 500 K/s. After the quenching process, the sample was amorphous and transparent. In a next step the amorphous sample was crystallized by annealing it for 6 h at 1273 K in air. The resulting material had grain sizes between 5 and 10 nm. Owing to the small grain size and dense structure the quenched bead was still transparent.

Another technique that was tested was the production of small amorphous samples of around 100 µm using water-quenched steel rollers [9], by the means of shock waves [10] or by flame spraying into distilled water to solidify amorphous beads [11, 12]. The flame spraying method had also been used by Rosenflanz *et al.* [13, 14] with eutectic compositions in the binary system Al_2O_3-RE_2O_3 as well as the ternary system Al_2O_3-RE_2O_3-ZrO_2. The crystallization behavior was investigated using DTA analysis. The gap between the glass transition (T_g) and crystallization temperatures (T_x) – termed the kinetic window – was found to be around 50 to 80 K depending on the type of the rare earth oxide and increased from Y to La. Within this temperature gap, densification occurred by viscous flow to obtain a dense bulk glass, which was still transparent and amorphous. The following anneal above T_x led to crystallization with a resulting crystal size of several nanometers to 100 nm, depending on the temperature. Furthermore the mechanical properties – hardness and fracture toughness – were measured.

Prnová *et al.* investigated Al_2O_3-Y_2O_3 microspheres prepared by means of flame synthesis [15, 16]. The method

* Corresponding author: carina.oelgardt@tu-clausthal.de

was similar to the method used by Rosenflanz *et al.* In their paper they described the cooling rate as 10^3 K/s [13]. This cooling rate is necessary to avoid crystallization in the quenched Al_2O_3-RE_2O_3 systems and achieve amorphous samples, whereas alumina, as a reluctant glass former, needs about 10^7 K/s.

Prnová reported that their flame-sprayed samples were partially crystallized, apart from the eutectic composition Al_2O_3-YAG, which was completely amorphous. As with Rosenflanz's results, the microspheres were transparent in visible light.

The kinetic window was determined to be 50 K for the eutectic composition, which is in agreement with Rosenflanz's results. Unlike Rosenflanz's results, densification within this gap did not lead to an amorphous, transparent bulk glass but to white, opaque samples with a primary YAG phase.

The aim of this research was the fabrication of amorphous microspheres in the Al_2O_3-Y_2O_3-ZrO_2 system using a CO_2 laser instead of a flame as an energy source.

In the field of ceramic research, lasers have been used in the past [17], for example, for sintering surfaces [18–20], for laser ablation [21,22] or for creating ceramic parts with various rapid prototyping techniques [23,24]. Compared to flame spraying, the laser technique offers some significant advantages, such as a high-purity energy source and the possibility of working without generating too much heat in a clean room [25].

In the Al_2O_3-Y_2O_3-ZrO_2 system, lasers have been used to modify the surface layer of eutectic compositions to improve fracture toughness and strength, especially in the high temperature range [26–29].

This article explains for the first time the laser process to produce microspheres in this material system. The resulting microspheres as well as their crystallization behavior will be discussed.

II. Experimental

The starting materials were 1.8 µm Al_2O_3 (Nabaltec AG, Schwandorf, Germany) with a purity of 99.7 %, 1.1 µm Y_2O_3 (Treibacher Industrie AG, Althofen, Austria) with a purity of 99.99 % and 0.3 µm ZrO_2 (Treibacher Industrie AG, Althofen, Austria) with a purity of 99.95 %.

The three powders were homogeneously mixed by means of milling with zirconia milling media in ethanol for 24 h. The suspension was dried under continuous stirring on a heat plate and stored in a drying furnace. After the powder was completely dry, it was sieved through a 125-µm screen.

Two different powder types were used as the source powders for the laser process:

a) Dried and sieved powder with the phases Al_2O_3, Y_2O_3 and ZrO_2 in the eutectic composition
b) Powders calcined at 1500 °C for 4 h after the first sieving step to pre-react the starting powders to Al_2O_3, YAG and YSZ (as determined with XRD), followed by a second sieving step.

The laser used for the experiments is a 5000 W CO_2 laser (Trumpf GmbH, Germany). A schematic of the experimental setup is shown in Fig. 1.

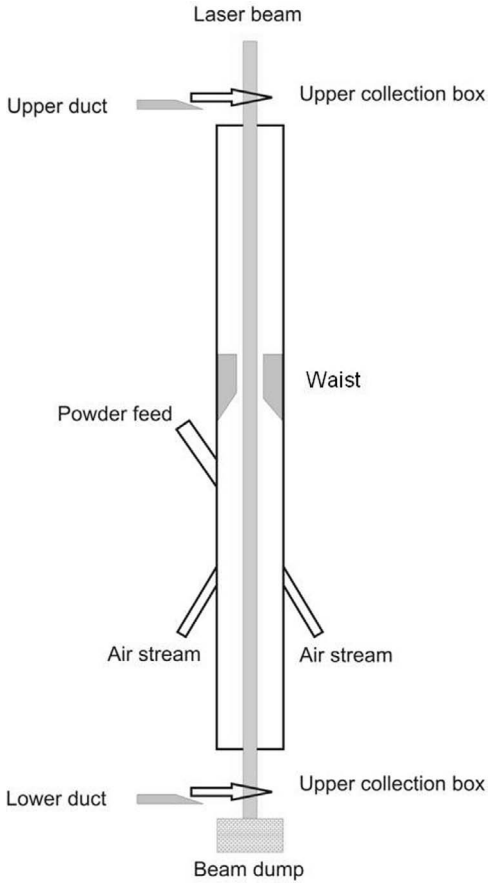

Fig. 1: Schematic of the experimental setup.

The laser beam passes down the center of a glass tube which has five inlets. One inlet is for powder feeding. A vibratory chute is used to get the particle through the inlet into the laser beam. The other four inlets provide an air stream in the opposite direction to the powder feed. The powder particles form agglomerates as they pass the vibratory chute and the powder inlet. Agglomerates smaller than a specific size follow the airstream through the upper duct and are collected in the upper collection box. Bigger agglomerates fall down and are collected in the lower collection box.

The cooling rates in the process are very high (~ 10^6 K/s), which is mainly a result of the beam profile. Since the laser does not directly generate heat like other energy sources (flames or furnaces), room temperature can be maintained next to the reaction zone.

In order to determine the effect of laser power on the resulting beads, the starting powders were exposed to laser powers in the range of 20 up to 100 %.

The resulting microspheres were cleaned ultrasonically in ethanol. Subsequently, a laser granulometer (LS230, Beckman Coulter Inc, USA) was used to measure the bead diameters, XRD (Diffractometer Siemens D5000 Kristalloflex, Germany) to determine the crystalline phases as well as the fraction of amorphous material and DSC (Netzsch DSC 404, Germany) with a heating rate of 10 K/min to study the crystallization behavior. Optical and scanning electron microscopy (Helios NanoLab 600, FEI, the Netherlands) were used to analyze the appearance and the microstructures of the microspheres.

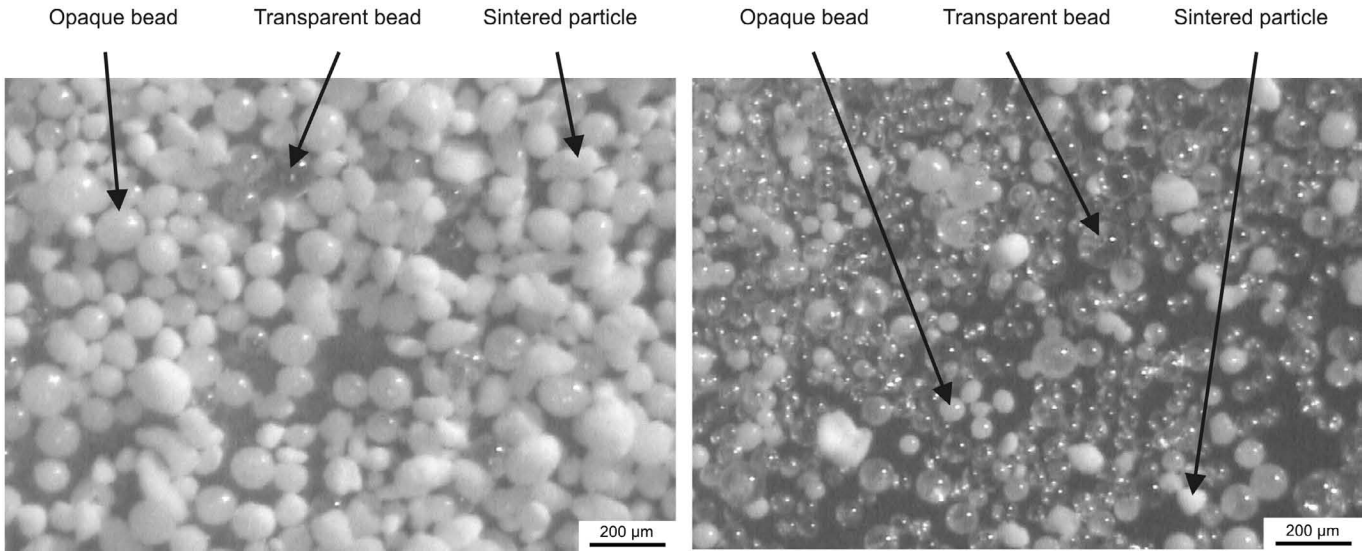

Fig. 2: Influence of the laser power on the optical appearance of the laser-treated powders; Left: 20 % of the laser power; Right: 100 % of the laser power.

Based on DSC results, the microspheres were heat-treated to induce crystallization. The annealed microspheres were then embedded in epoxy resin, ground and polished to analyze the microstructure with an SEM.

III. Results and Discussion.

To determine the influence of laser energy on the microbead characteristics, the laser power was varied from 20 % up to 100 % for a series of powder samples.

After cleaning, the resulting samples were first observed by means of optical microscopy.

With a laser power of 20 % (1000 W), the laser-treated powder contained mostly opaque beads as well as sintered powder particles and just a few transparent beads. With increasing laser power, the amount of transparent beads increased (see Fig. 2). Even at the maximum laser power the samples contain opaque beads and a few sintered particles.

The laser-treated powders were analyzed by means of XRD to determine their amorphous content using ZnO as an internal standard [30]. Fig. 3 shows that the amorphous phase content increases with laser power.

An average amorphous content of 74.5 % ± 2.3 % was measured in samples treated with the maximum laser power (calculated from five samples).

The residual crystalline phases are Al_2O_3, $Y_3Al_5O_{12}$ (YAG), yttria-stabilized zirconia (YSZ), Y_2O_3, ZrO_2 and $YAlO_3$ (YAP). After conventional sintering, the three starting materials form Al_2O_3, YAG and YSZ [31]. Cooling the eutectic mixture from the melt slowly enough for crystallization to occur also resulted in complete phase reaction to Al_2O_3, YAG and YSZ [26]. This result leads to the conclusion that either the time or temperature was not sufficient to complete the reaction. Therefore a calcination step to pre-react the starting powders was integrated into the process. Four hours at 1500 °C were found to be sufficient for complete phase formation. Fig. 4 shows a comparison between a conventional sintered sample (Fig. 4A) and the pre-calcined starting powder for the laser process (Fig. 4B).

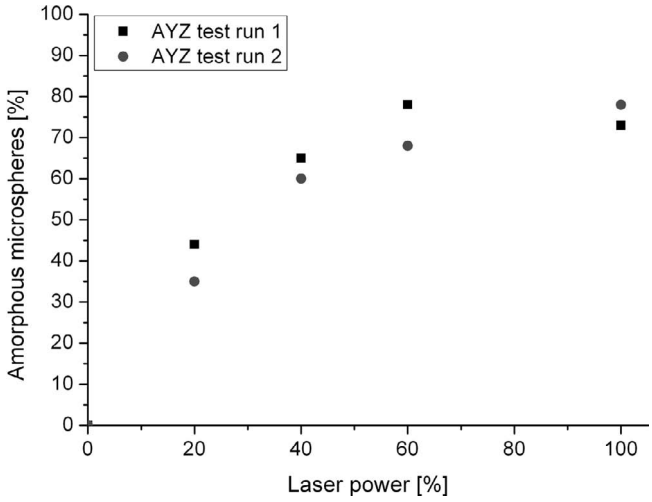

Fig. 3: Amorphous content in the laser-treated powders as a function of laser power.

For the experiments with the calcined powder a maximum laser power of 5000 W has been used because with this laser power the highest amorphous amounts with the uncalcined material have been achieved. The amount of amorphous particles could be increased from 74.5 % ± 2.3 % with the uncalcined starting powder to 84.3 % ± 1.1 % in case of the calcined starting powder.

Fig. 5 shows a comparison of XRD spectra taken from the microspheres produced with uncalcined starting powder (Fig. 5A) and the pre-calcined starting powder (Fig. 5B).

As was mentioned above, the microspheres produced with the uncalcined starting powder contained residual crystalline phases of Al_2O_3, YAG, yttria-stabilized zirconia (YSZ), Y_2O_3, ZrO_2 and YAP. In comparison the microspheres produced from the pre-calcined starting powder contained just Al_2O_3, YAG and YSZ.

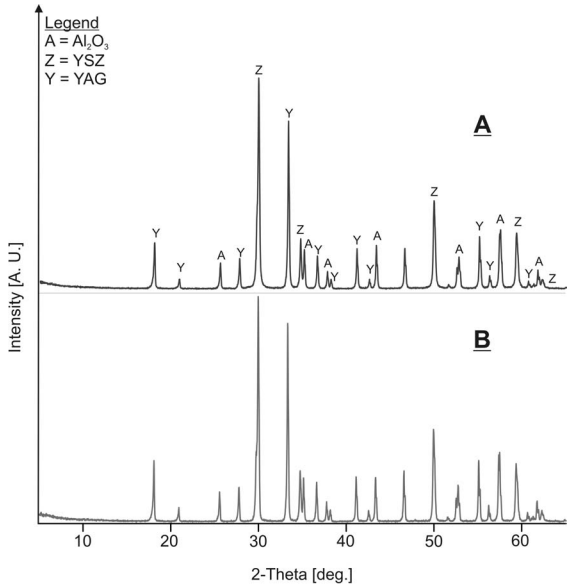

Fig. 4: XRD patterns of A: conventional sintered sample [31], B: pre-calcined starting powder.

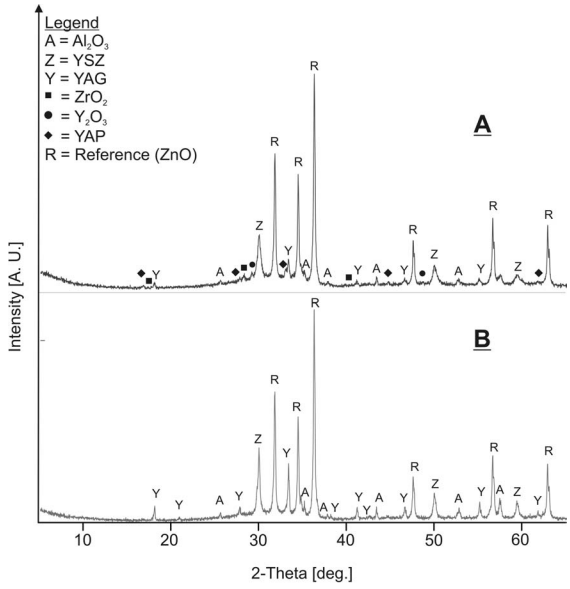

Fig. 5: XRD patterns of microspheres produced from A: uncalcined starting powder, B: pre-calcined starting powder.

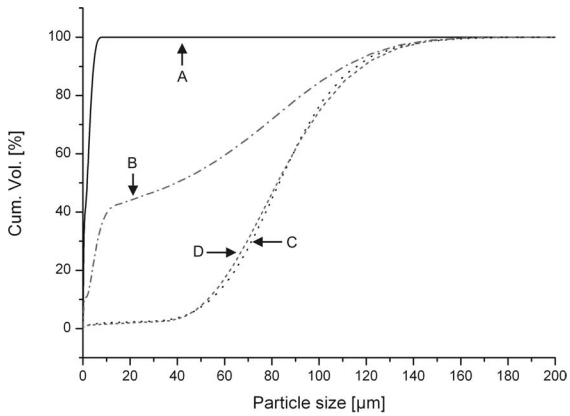

Fig. 6: Comparison of particle sizes of the A: uncalcined starting material (continuous line), B: pre-calcined starting material (dashed-dotted line), C: microspheres made from uncalcined material (dotted line), D: microspheres made from pre-calcined material (dashed line).

Fig. 6 shows the particle size distribution of the starting material and the laser-produced microspheres. The uncalcined starting material has a D_{50} particle size of 1.2 µm (Fig. 6A) and the calcined starting material of 42 µm (Fig. 6B). After the laser process (Figs. 6C and D) both types of microspheres formed by means of laser fusing have a D_{50} particle size of ~ 85 µm. It is apparent to see that the resulting size of the microspheres is not dependent on the particle size of the starting material but may be caused by agglomeration of the powders during the feeding process and the flow conditions in the glass tube during laser fusing.

It was not possible to increase the amorphous amounts to 95 % or more as was shown in earlier studies with the ternary [13,14] or the binary eutectic Al_2O_3-YAG [15,16].

The problem in the present work may be the beam profile. The laser that was used for the experiments has a ring profile (see Fig. 7 [32]), which leads to an area of zero intensity in the middle of the laser beam.

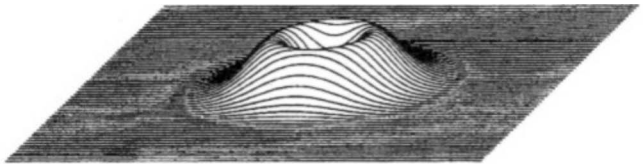

Fig. 7: Ring profile of the laser beam used for these experiments [32].

Owing to this area in the middle of the beam, the temperature profile experienced by the powders is inhomogeneous. Therefore some powder particles may pass through the process without undergoing sufficient temperature/cooling treatment. These particles are either just sintered or appear as opaque microspheres. Neither type of particle can be removed by cleaning ultrasonically in ethanol and therefore affects the amount of amorphous material.

Fig. 8 shows a transparent and an opaque bead as well as a sintered particle.

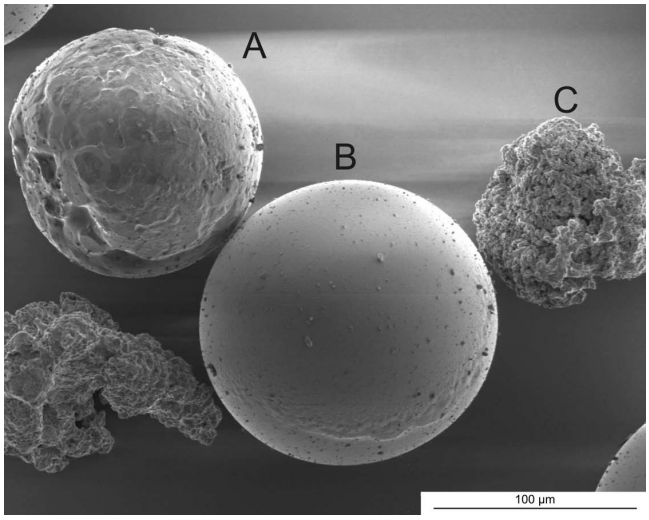

Fig. 8: Particles after the laser treatment (SEM, SE) A: opaque microsphere, B: transparent microsphere, C: sintered particle.

The opaque beads have a rough surface while the surface of the transparent beads is very smooth. The particles that are just sintered are not formed into beads like the other two types (Fig. 9).

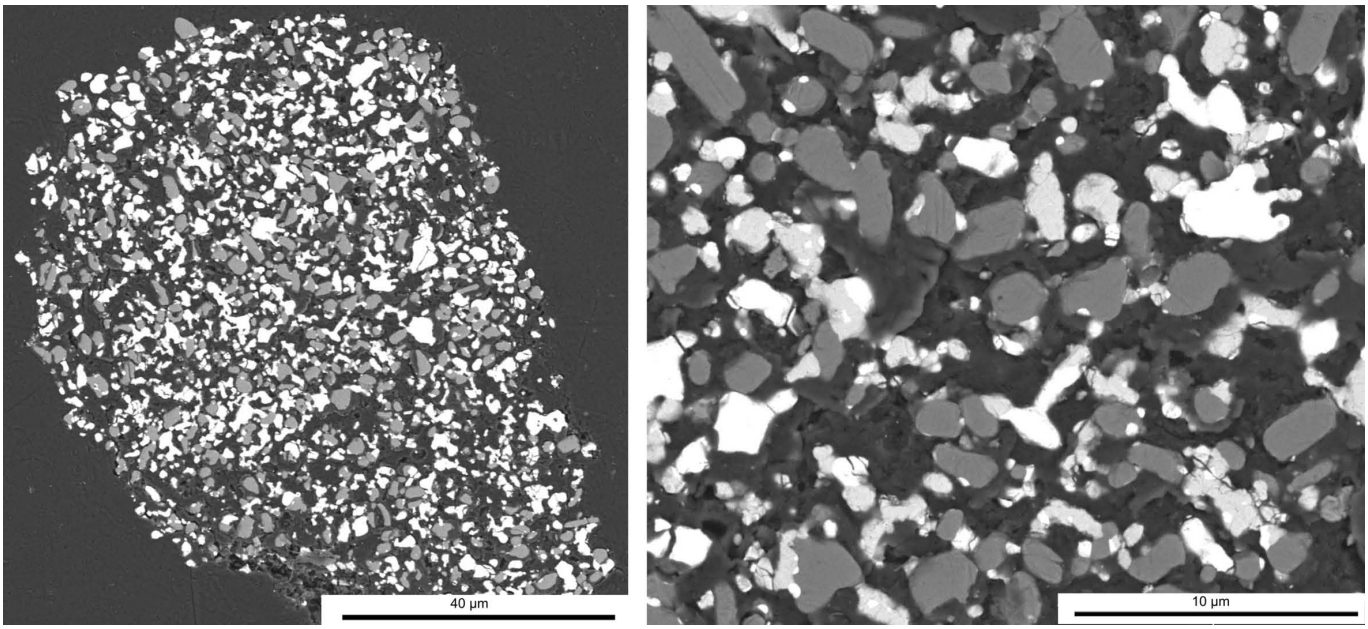

Fig. 9: Cross-section of sintered particles (polished, SEM, BSE, C-coated), Black: Al_2O_3 Gray: YAG, White: YSZ.

The opaque microspheres show a wide variety of microstructures, which may result from the inhomogeneous temperature treatment caused by the ring-profile of the laser beam.

Fig. 10 shows four examples of generated microstructures in the opaque beads.

The microstructure of the transparent beads is shown in Figs. 11A and 11B.

All of the transparent beads have a crystalline surface layer with an average thickness of 1.8 µm ± 0.7 µm. Furthermore a crystalline layer also appears on pores within a transparent bead. These crystalline layers show a structure typical for a eutectic that has been solidified from the melt. Also, the dendritic growth of the crystallites could arise from a composition near the surface different from that of the bulk. Then, crystallization proceeds as long as the amorphous material near the surface with this unique composition is consumed. The composition of the black phase is equal to alumina, the gray phase YAG and the white phase YSZ. The inner area of the bead is amorphous. In spite of the crystalline layer the beads are transparent. This may be explained by the dense and fine structure of the layer. Previous papers [13–16] also reported transparent beads but a crystalline layer in the surface near region of the beads has not been discussed. It is unknown whether the crystalline layer is a feature intrinsic to the laser process or is always present at the surface of this type of transparent beads.

The resulting microspheres after the laser treatment produced at 100 % of the laser power (including opaque beads and sintered particles) have been analyzed by means of DSC (see Fig. 12).

The uncalcined starting material does not show any reaction in the temperature range up to 1300 °C. The laser-treated microspheres show two exotherms at 910 °C and 1200 °C. Rosenflanz *et al.* published their DSC data on the binary and ternary systems Al_2O_3-RE_2O_3(-ZrO_2). The DSC diagram for Gd as a rare earth (RE) material, also showing two exothermic peaks, can be found in their paper [13]. References 13 and 33 suggest that the first peak is caused by nucleation and growth of a crystalline phase from solid solution, likely YAG or a mixture of $YAlO_3$ (YAP) and alpha-Al_2O_3 and the second peak by a polyamorphic transition from a metastable high-density amorphous phase, which cannot crystallize, to a more stable low-density amorphous phase. In the present paper the glass transition temperature T_g can be observed at around 885 °C and crystallization at T_x = 910 °C. In comparison to Rosenflanz's results, glass transition occurs at the same temperature, but the onset temperature of crystallization is about 10 °C lower, which leads to a smaller kinetic window.

On the other hand, it is also possible that rapid quenching has formed a metastable high-density amorphous solid with a T_g at 885 °C. After T_g it converts into a more stable amorphous phase with lower density, giving rise to the first exotherm at 910 °C. Then, the slight undulation seen at 1125 °C could be interpreted as the T_g of the low-density amorphous phase, with the broad second exotherm around 1200 °C resulting from its crystallization. This model could explain the following microstructural changes observed upon annealing transparent beads:

Based on the DSC results, transparent microspheres (produced at 100 % laser power) have been annealed to the following temperatures at the same heating rate as in the DSC run: 900 °C, 1000 °C, 1150 °C, 1200 °C, 1250 °C and 1300 °C (Figs. 13A – 13F).

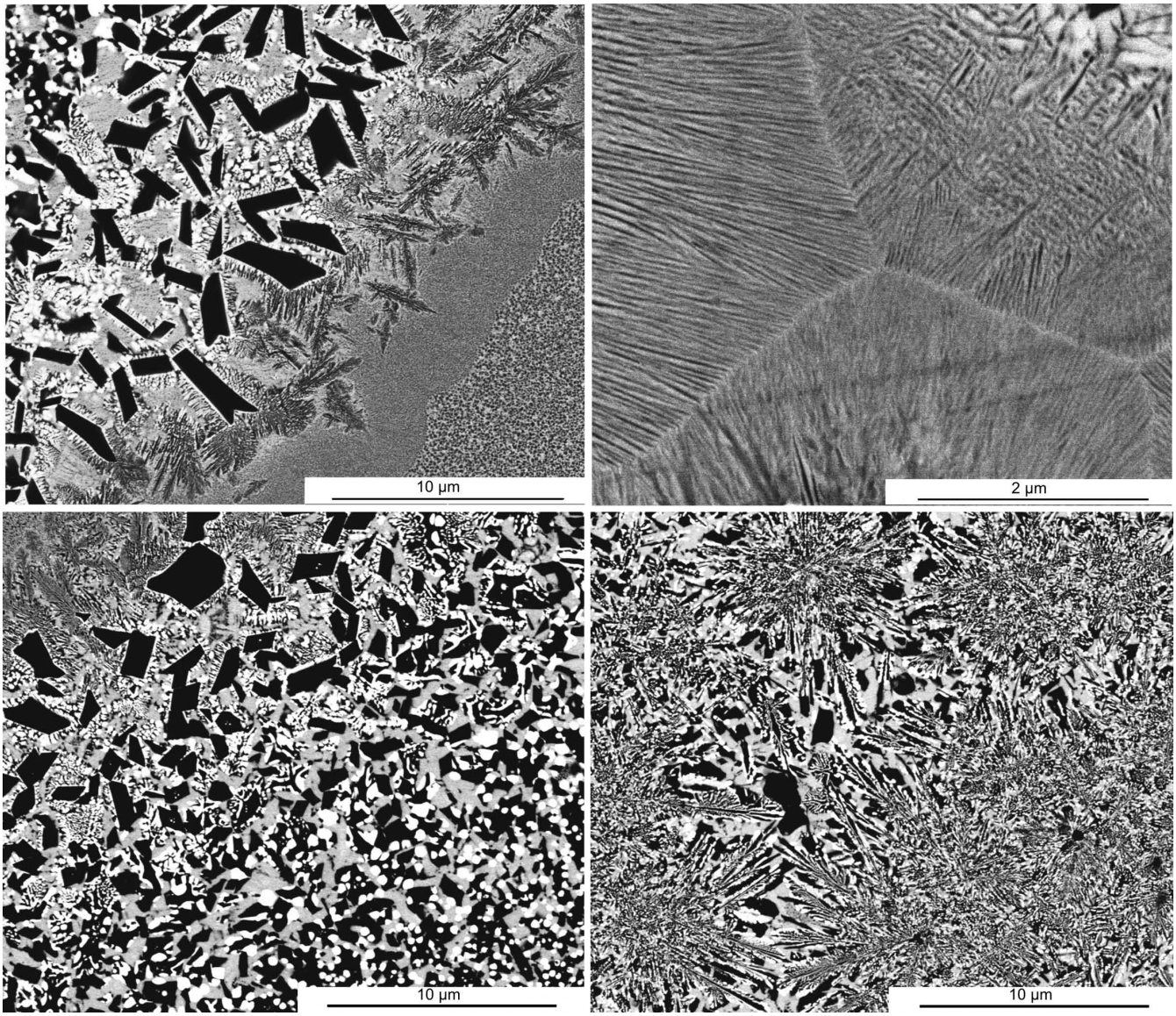

Fig. 10: Generated microstructures of opaque beads after laser treatment (cross-section, polished, SEM, BSE, C-coated).

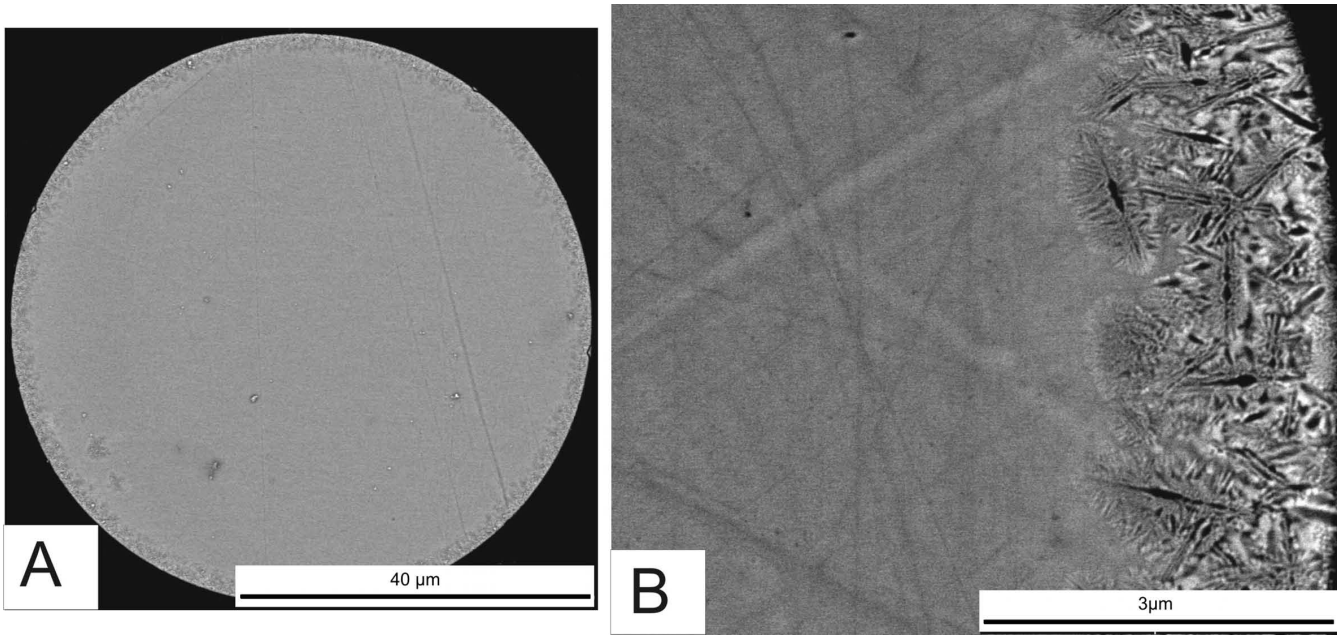

Fig. 11: Generated microstructures of transparent beads after laser treatment (cross-section, polished, SEM, BSE, C-coated).

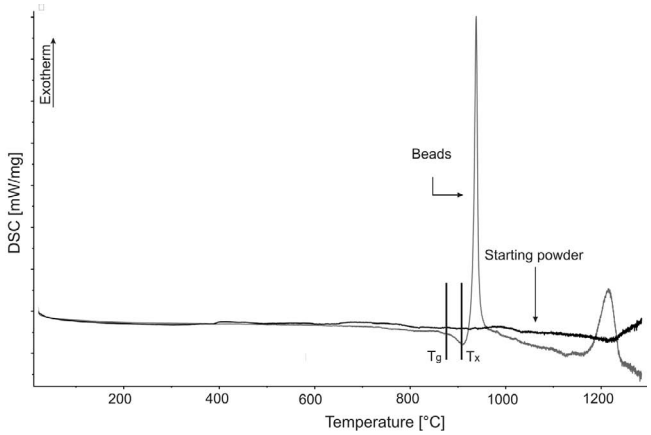

Fig. 12: DSC analysis of the laser-treated microspheres (red curve); the black curve shows as a comparison the uncalcined starting material.

According to references 13 and 33 and the DSC measurement shown in Fig. 12, crystallization would occur between 900 °C and 1000 °C. In this temperature range no change in the microstructure is observed. After heating to temperatures above 1200 °C (up to 1300 °C) significant changes, accompanied by the formation of distinct phase, become visible in SEM. These observations support the viewpoint that the first exotherm in Fig. 12 at 910 °C originates from a polyamorphic transition and the second broad one at 1200 °C from crystallization of the transparent beads.

Though they are obviously crystalline at 1300 °C, the beads stay transparent during the entire annealing procedure. Furthermore, the crystalline surface layer seems to be stable and was not observed to grow during annealing of the transparent microspheres.

IV. Conclusion

This paper reports for the first time on the production of Al_2O_3-Y_2O_3-ZrO_2 eutectic microspheres using a CO_2 laser. Though there are still process improvements to be made, this new technique offers advantages (i.e. high-purity energy source, defined beam profile) in comparison with techniques reported previously. A yield of 85 % amorphous in the laser-treated microspheres has been achieved.

The influence of the starting powder – not uncalcined and pre-calcined – and the laser power on the resulting microspheres has been investigated. Furthermore, the microspheres have been analyzed by means of XRD and DSC to obtain information about the amorphous character and the residual crystalline phases. Single transparent beads have been separated for closer investigation of the effects of heat treatment on the microstructure and residual amorphous phase content. It was found that the crystalline surface layer does not grow during heat treatment whereas the inside area of the beads changes from amorphous to crystalline owing to volume crystallization. In spite of the obvious crystalline character after heat treatment, the beads are still transparent.

Owing to the fact that the beads are transparent after crystallization it can be assumed that it will be possible to get a transparent ceramic in this material system, which will be explored in later experiments.

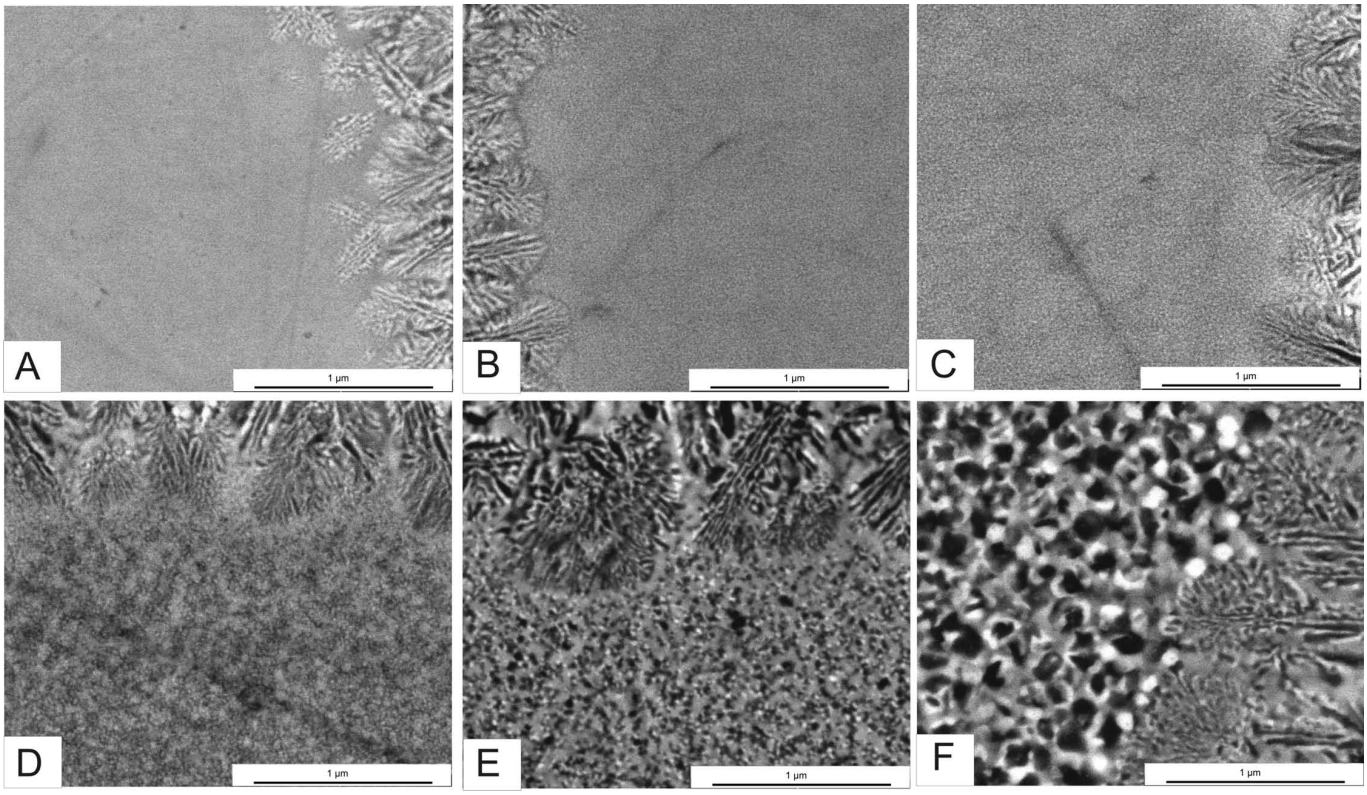

Fig. 13: Cross-sections of transparent microspheres (polished, SEM, BSE, C-coated) annealed at A: 900 °C, B: 1000 °C, C: 1150 °C, D: 1200 °C, E: 1250 °C, F: 1300 °C.

References

1 Ikesue, A., Kamata, K.: Microstructure and optical properties of hot isostatically pressed Nd:YAG ceramics, *J. Am. Ceram. Soc.*, **79**, 1927 – 1933, (1996).

2 Gilde, G., Patel, P., Patterson, P., Blodget, D., Duncan, D., Hahn, D.: Evaluation of hot pressing and hot isostatic pressing parameters on the optical properties of spinel, *J. Am. Ceram. Soc.*, **88**, 2747 – 2751, (2005).

3 Itatani, K., Tsujimoto, T., Kishimoto, A.: Thermal and optical properties of transparent magnesium oxide ceramics fabricated by post hot-isostatic pressing, *J. Eur. Ceram. Soc.*, **26**, 639 – 645, (2006).

4 Salman, S.M., Salama, S.N., Abo-Mosallam, H.A.: Crystallization behaviour and properties of multicomponent strontium-containing lithia calcia silicate glasses, *Ceram. Int.*, **36**, 2307 – 2314, (2010).

5 El-Kheshen, A.A., Zawrha, M. F.: Sinterability, microstructure and properties of glass/ceramic composites, *Ceram. Int.*, **29**, 251 – 257, (2003).

6 Alekseeva, I., Dymshiths, O., Tsenter, M., Zhilim, A., Golubkov, V., Denisov, I., Skoptsov, N., Malyarevich, A., Yumashev, K.: Optical applications of glass-ceramics, *J. Non-Cryst. Sol.*, **356**, 3042 – 3058, (2010).

7 Boutarfaia, A., Legouera, M., Poulain, M.: Glass formation and crystallization kinetics in a multicomponent fluoride glass, *J. Non-Cryst. Sol.*, **291**, 176 – 180, (2001).

8 Araki, S., Yoshimura, M.: Transparent nano-composite ceramics by annealing of amorphous phase in the HfO_2-Al_2O_3-$GdAlO_3$ system, *Int. J. Appl. Ceram. Technol.*, **1**, 155 – 160, (2004).

9 MacDowell, J.F., Beall, G.H.: Immiscibility and crystallization in Al_2O_3-SiO_2 glasses, *J. Am. Ceram. Soc.*, **52**, 17 – 25, (1969).

10 Claussen, N., Lindemann, G., Petzow, G.: Rapid solidification in the Al_2O_3 - ZrO_2 system, *Ceram. Int.*, **9**, 83 – 86, (1983).

11 Thorne, D.J.: Glass formation in refractory oxide systems based on alumina, *Proc. Br. Ceram. Soc.*, **14**, 131 – 145, (1969).

12 Takamori, T., Roy, R.: Rapid crystallization of SiO_2-Al_2O_3 glasses, *J. Am. Ceram. Soc.*, **56**, 639 – 644, (1973).

13 Rosenflanz, A., Frey, M., Endres, B., Anderson, T., Richards, E., Schardt, C.: Bulk glasses and ultrahard nanoceramics based on alumina and rare-earth oxides, *Nature*, **430**, 761 – 764, (2004).

14 Rosenflanz, A., Frey, M., Endres, B., Anderson, T., Richards, E., Schardt, C.: Bulk glasses and glass-ceramics based on Al_2O_3, their processing methods and properties, *Glass Sci. Technol. C*, **78**, 27 – 32, (2005).

15 Prnová, A., Karell, R., Galusek, D.: Y_2O_3-Al_2O_3 binary glass microspheres: Synthesis and characterisation, *Adv. Mat. Res.*, **39 – 40**, 189 – 192, (2008).

16 Prnová, A., Karell, R., Galusek, D.: The preparation of binary Al_2O_3-Y_2O_3 glass microspheres by flame synthesis from powder oxide precursors, *Ceramics - Silikáty*, **52**, 109 – 114, (2008).

17 Samant, A.N., Dahotre, N.B.: Laser machining of structural ceramics - A review, *J. Eur. Ceram. Soc.*, **29**, 969 – 993, (2009).

18 Bertrand, P., Bayle, F., Combe, C., Goeuriot, P., Smurov, I.: Ceramic components manufacturing by selective laser sintering, *Appl. Surf. Sci.*, **254**, 989 – 992, (2007).

19 Ester, F.J., Merino, R.I., Pastor, J.Y., Martin, A., LLorca, J.: Surface modification of Al_2O_3-ZrO_2(Y_2O_3) eutectic oxides by laser melting: processing and wear resistance, *J. Am. Ceram. Soc.*, **91**, 3552 – 3559, (2008).

20 Gahler, A., Heinrich, J.G., Kawanowa, H., Schwertfeger, F., Günster, J.: Three-dimensional laser surface sintering of SiO_2 green bodies, *Int. J. Appl. Ceram. Technol.*, **3**, 331 – 335, (2006).

21 Hoon Kim, S., Sohn, I.-B., Jeong, S.: Ablation characteristics of aluminium oxide and nitride ceramics during femtosecond laser micromachining, *Appl. Surf. Sci.*, **225**, 9717 – 9720, (2009).

22 Sola, D., Escartin, A., Cases, R., Pena, J.I.: Laser ablation of advanced ceramics and glass-ceramic materials: Reference position dependence, *Appl. Surf. Sci.*, **257**, 5413 – 5419, (2011).

23 Tian, X., Günster, J., Melcher, J., Li, D., Heinrich, J.G.: Process parameters analysis of direct laser sintering and post treatment of porcelain components using Taguchi's method, *J. Eur. Ceram. Soc.*, **29**, 1903 – 1915, (2009).

24 Gahler, A., Heinrich, J.G.: Direct laser sintering of Al_2O_3-SiO_2 dental ceramic components by layer-wise slurry deposition, *J. Am. Ceram. Soc.*, **89**, 3076 – 3080, (2006).

25 Günster, J., Engler, S., Heinrich, J.G., Schwertfeger, F.: A novel route for the production of ultra pure SiO_2 crucibles, *Glass Sci. Technol.* , **78**, 18 – 22, (2005).

26 Lakiza, S.M.: Directionally solidified eutectics in the Al_2O_3-ZrO2-$Ln_8Y)_2O_3$ systems (Review), *Powder Metall. Met. Ceram.*, **48**, 42 – 59, (2009).

27 Pastor, J.Y., LLorca, J., Martín, A., Pena, J.I., Oliete, P.B.: Fracture toughness and strength of Al_2O_3-$Y_3Al_5O_{12}$ and Al_2O_3-$Y_3Al_5O_{12}$-ZrO_2 directionally solidified eutectic oxides up to 1900 K, *J. Eur. Ceram. Soc.*, **28**, 2345 – 2351, (2008).

28 Su, H., Zhang, J., Deng, Y., Liu, L., Fu, H.: A modified preparation technique and characterization of directionally solidified Al_2O_3/$Y_3Al_5O_{12}$ eutectic *in situ* composites, *Scripta mater.*, **60**, 362 – 365, (2009).

29 Oliete, P.B., Pena, J.I., Larrea, A., Orera, V.M., LLorca, J., Pastor, J.Y., Martin, A., Segurado, J.: Ultra-high-strength nanofibrillar Al_2O_3-YAG-YSZ eutectics, *Adv. Mater.*, **19**, 2313 – 2318, (2007).

30 Westphal, T., Füllmann, T., Pöllmann, H.: Rietveld quantification of amorphous portions with an internal standard - Mathematical consequences of the experimental approach, *Powder Diffr.*, **24**, 239 – 243, (2009).

31 Oelgardt, C., Anderson, J., Heinrich, J.G., Messing, G.L.: Sintering, microstructure and mechanical properties of Al_2O_3-Y_2O_3-ZrO_2 (AYZ) eutectic composition ceramic microcomposites, *J. Europ. Ceram. Soc.*, **30**, 649 – 656, (2010).

32 Herziger, G., Loosen, P.: Materials processing with lasers (in German), Hanser Verlag, Munich - Vienna (1993).

33 Wilding, M.C., McMillan, P.F.: Polyamorphic transition in yttria-alumina liquids, *J. Non-Cryst. Sol.*, **293 – 295**, 357 – 365, (2001).